Supplementary Material

Primers used in H3K27ac ChIP-qPCR

IGF2-R-1	For: 5'-CACCGCGTCAACATACCAGG-3'	Positive control Cai Y, et al., Nat Commun. 2021
	Rev: 5'-CATGTGTGATTCGTGCCTTGC-3'	
IGF2-R-2	For: 5'-AAGCAAGGAAGTCACGGGTC-3'	
	Rev: 5'-GAGAAATAGGGCTTCGGGCG-3'	
CDKN1A-e-1	For: 5'-GACTGGTGCTGGCTGAAAGG-3'	
	Rev: 5'-TTCCAAGGCTGGGTCATAAA-3'	
CDKN1A-e-2	For: 5'-TTGTTGCCTGTTGTTCCAAT-3'	
	Rev: 5'-GAGCACCAATAATGCCTCTT-3'	
CDKN1A-e-3	For: 5'-TTGTTGCCTGTTGTTCCAAT-3'	
	Rev: 5'-GAGCACCAATAATGCCTCTT-3'	
CDKN1A-e-4	For: 5'-ACGAGCCCTCAGTCTTCTTG-3'	
	Rev: 5'-GGAGATACCACCACTGTCAAA-3'	
CDKN1A-e-5	For: 5'-AAGATGGCTATGTCGGTGAA-3'	
	Rev: 5'-CTGGGTCTGATATGAAACTCG-3'	
IGF2-R-3	For: 5'-GGGCATCTCTGTCATGGTGG-3'	Positive control Cai Y, et al., Nat Commun. 2021
	Rev: 5'-GGCATTTGGGATACACCCGT-3'	
IGF2-R-4	For: 5'-GCGAGGTAAACCTCCCAGAG-3'	
	Rev: 5'-CGGGTCTGGTGATGCCATAG-3'	
EMP1-e-1	For: 5'-GAAAGGAAAGGGAAGGAATA-3'	
	Rev: 5'-CAAGAAGTCTACTAAGGCAGGT-3'	
EMP1-e-2	For: 5'-CTTTCTATGGCACCACTCTG-3'	
	Rev: 5'-GTTTCCACGCCTACTACCTG-3'	
EMP1-e-3	For: 5'-GAAGGTATAACATGGTCGTG-3'	
	Rev: 5'-TTGGGAATCATAATAGCAAC-3'	
EMP1-e-4	For: 5'-GCAGGTCCCAGTGAGTGTTG-3'	
	Rev: 5'-TCATGGATGGAGCTGAAAGC-3'	
EMP1-e-5	For: 5'-GGCTGGGAGTAGGAGATGGG-3'	
	Rev: 5'-GGAGGCAGAAGTGGGAGGAT-3'	

Primers used in TEAD4 ChIP-qPCR

CTGF	For: 5'-CTGGCAATGTCCTGACAAAA-3'	Positive control, Guo Y, et al., Nat Commun. 2022
	Rev: 5'-CTGGCTGATCTCAAGTGCTG-3'	
CXCL1-e	For: 5'-CATTCGTAACTATTAGGGACT-3'	
	Rev: 5'-GTGAAAGAGGAGGAACAAGG-3'	
CXCL2-e	For: 5'-GAATGAATCCTGGAGCTGTT-3'	
	Rev: 5'-GTTTAGTCTTGGGAGGGTGT-3'	
CXCL5-e	For: 5'-GGTCTGGCAGTCCAATGAAG-3'	
	Rev: 5'-GGGCTCACTGATTTGCTCCT-3'	
IL6-e	For: 5'-TATTCCACATTGGTGCTTAC-3'	
	Rev: 5'-GTCTGGTTGTATCTCCCTCA-3'	
IGFBP1-e	For: 5'-CTGGATGAAGGGACTGTGGT-3'	
	Rev: 5'-ATTCTTCTTGGATGTGGGAG-3'	
IGFBP2-e	For: 5'-CAGGCTGCTCTTGAACTCAT-3'	
	Rev: 5'-GTCCACCCACTCTGCTTACT-3'	
CXCL8-e	For: 5'-TGCCACTGTATCCTAACCTG-3'	
	Rev: 5'-ATTTGTCTCACCCACTTGAC-3'	
MMP9-e	For: 5'-AAAGTCAGGCATCAGTATTCAA-3'	
	Rev: 5'-GGTATAACAAGTGTCTCGTGGG-3'	
CCL2-e	For: 5'-GACTATCTGGGTGGGTAGGG-3'	
	Rev: 5'-AGAGGACTGGCGTAGAGGTT-3'	
CCL3-e	For: 5'-TAGGTACAGAATGATAGGGCAATT-3'	
	Rev: 5'-TCTTGAATCTGGGAGGTGGA-3'	
CCL7-e	For: 5'-CCACCAACAGTAAACAAAGA-3'	
	Rev: 5'-GTATCACCTCACCTCCATTA-3'	
SPP1-e	For: 5'-TTGAGATGGGAGACAAGAAA-3'	
	Rev: 5'-TAGCATAGCACCGATGAAGC-3'	

Primers used in RT-qPCR

CDKN2A	For: 5'-GATCCAGGTGGGTAGAAGGTC-3'
	Rev: 5'-CCCCTGCAAACTTCGTCCT-3'
CDKN1A	For: 5'-TGTCCGTCAGAACCCATGC-3'
	Rev: 5'-AAAGTCGAAGTTCCATCGCTC-3'
EMP1	For: 5'-GTGCTGGCTGTGCATTCTTG-3'
	Rev: 5'-CCGTGGTGATACTGCGTTCC-3'
TEAD1	For: 5'-ATGGAAAGGATGAGTGACTCTGC-3'
	Rev: 5'-TCCCACATGGTGGATAGATAGC-3'
TEAD2	For: 5'-CTTCGTGGAACCGCCAGAT-3'
	Rev: 5'-GGAGGCCACCCTTTTTCTCA-3'
TEAD3	For: 5'-TGGACCCTCTCAGGACATCAA-3'
	Rev: 5'-CCAGGGGCTCATAACTGCTG-3'
TEAD4	For: 5'-GAACGGGGACCCTCCAATG-3'
	Rev: 5'-GCGAGCATACTCTGTCTCAAC-3'
CXCL1	For: 5'-TGCTGCTCCTGCTCCTGGTA-3'
	Rev: 5'-TGTGGCTATGACTTCGGTTTGG-3'
CXCL5	For: 5'-AGCTGCGTTGCGTTTGTTTAC-3'
	Rev: 5'-AGCTGCGTTGCGTTTGTTTAC-3'
IL6	For: 5'-ACTCACCTCTTCAGAACGAATTG-3'
	Rev: 5'-CCATCTTTGGAAGGTTCAGGTTG-3'
IGFBP1	For: 5'-TTTTACCTGCCAAACTGCAACA-3'
	Rev: 5'-CCCATTCCAAGGGTAGACGC-3'
IGFBP2	For: 5'-TGCACATCCCCAACTGTGAC-3'
	Rev: 5'-TGTAGAAGAGATGACACTCGGG-3'
CXCL8	For: 5'-ACTGAGAGTGATTGAGAGTGGAC-3'
	Rev: 5'-AACCCTCTGCACCCAGTTTTC-3'
MMP9	For: 5'-AGACCTGGGCAGATTCCAAAC-3'
	Rev: 5'-CGGCAAGTCTTCCGAGTAGT-3'
CCL2	For: 5'-CAGCCAGATGCAATCAATGCC -3'
	Rev: 5'-TGGAATCCTGAACCCACTTCT-3'
CCL7	For: 5'-CAGCTGCTTTCAGCCCCCAGGGGCT-3'
	Rev: 5'-TGGCTACTGGTGGTCCTTCT-3'
SPP1	For: 5'-GAAGTTTCGCAGACCTGACAT-3'
	Rev: 5'-GTATGCACCATTCAACTCCTCG-3'
GAPDH	For: 5'-GACTAACCCTGCGCTCCTG-3'
	Rev: 5'-GCCCAATACGACCAAATCAG-3'

siRNA sequence used in knock down expriment

siTEAD4 #1	5′-GGAACAAACUGUGCCUGAATT-3′
siTEAD4 #2	5′-GCUUGUGGAUGAAGUUGATTT-3′

Antibodies

TEAD4	Proteintech	12418-1-AP
IgG	Proteintech	30000-0-AP
Anti-rabbit IgG H&L	Abcam	ab205718
H3K27ac	Abcam	ab4729
Goat anti-Rabbit IgG (H+L) Highly Cross-Adsorbed Secondary Antibody, Alexa Fluor 488	Invitrogen	Cat# A-11034
Ki-67	Abcam	ab15580
IRDye 800CW anti-mouse	LI-COR	926-32210
IRDye 800CW anti-rabbit	LI-COR	92632211
P16	Proteintech	10883-1-AP
β-actin	Abcam	ab8226

SUPPLEMENTARY FIGURES AND LEGENDS

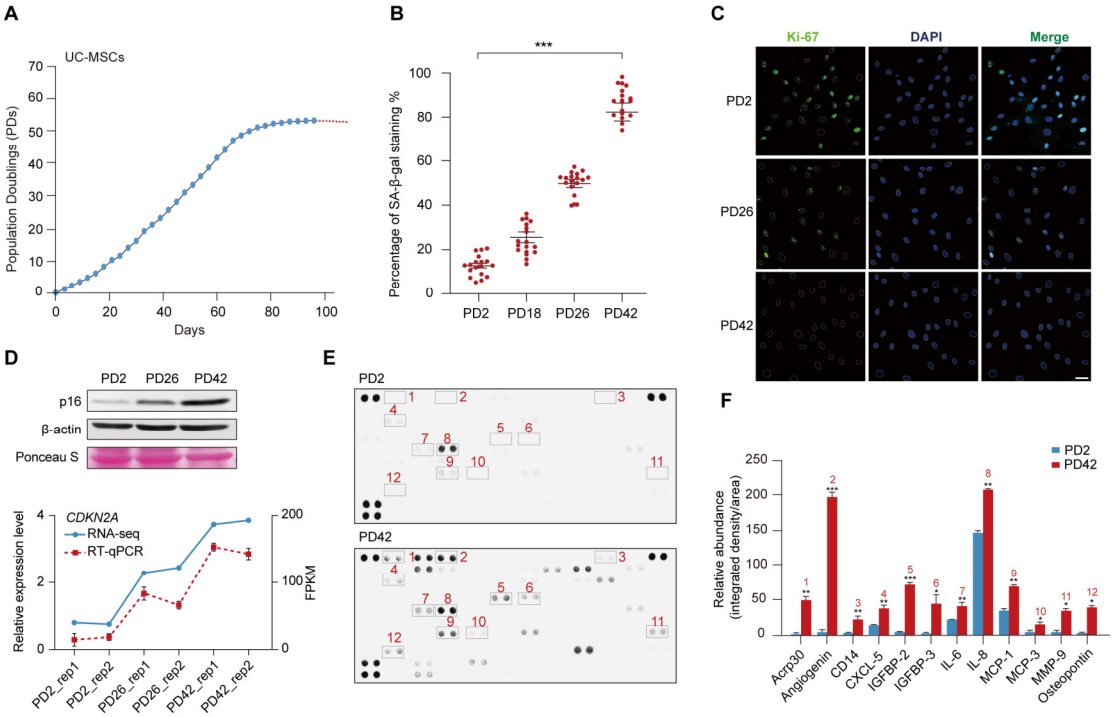

Supplementary Figure S1. Creation of an *in vitro* replicative senescence model. (A) Population doubling of primary human umbilical cord mesenchymal stem cells (UC-MSCs). (B) Percentage of SA-β-gal staining in young to senescent UC-MSCs. Error bars indicate the mean ± S.E.M. of three independently performed experiments. ***$p < 0.001$. A Student's *t*-test was used for statistical analysis. (C) Immunofluorescence staining of Ki-67 in UC-MSCs. The nucleolus is indicated by DAPI staining. Scale bar, 10 μm. (D) Top: Immunoblotting of P16 expression in young to senescent UC-MSCs. β-actin and ponceaus S were used as the loading controls. Bottom: *CDKN2A* expression in PD2, PD26, and PD42 UC-MSCs. The dashed line indicates RT-qPCR, while the solid line indicates RNA-seq data. Error bars indicate the mean ± S.E.M. of three independently performed experiments. (E and F) Cytokine array analysis of secreted proteins and relative quantitation of SASP factors during senescence. Error bars indicate the mean ± S.E.M of three independently performed experiments. *$p < 0.05$, **$p < 0.01$, ***$p < 0.001$. A Student's *t*-test was used for statistical analysis.

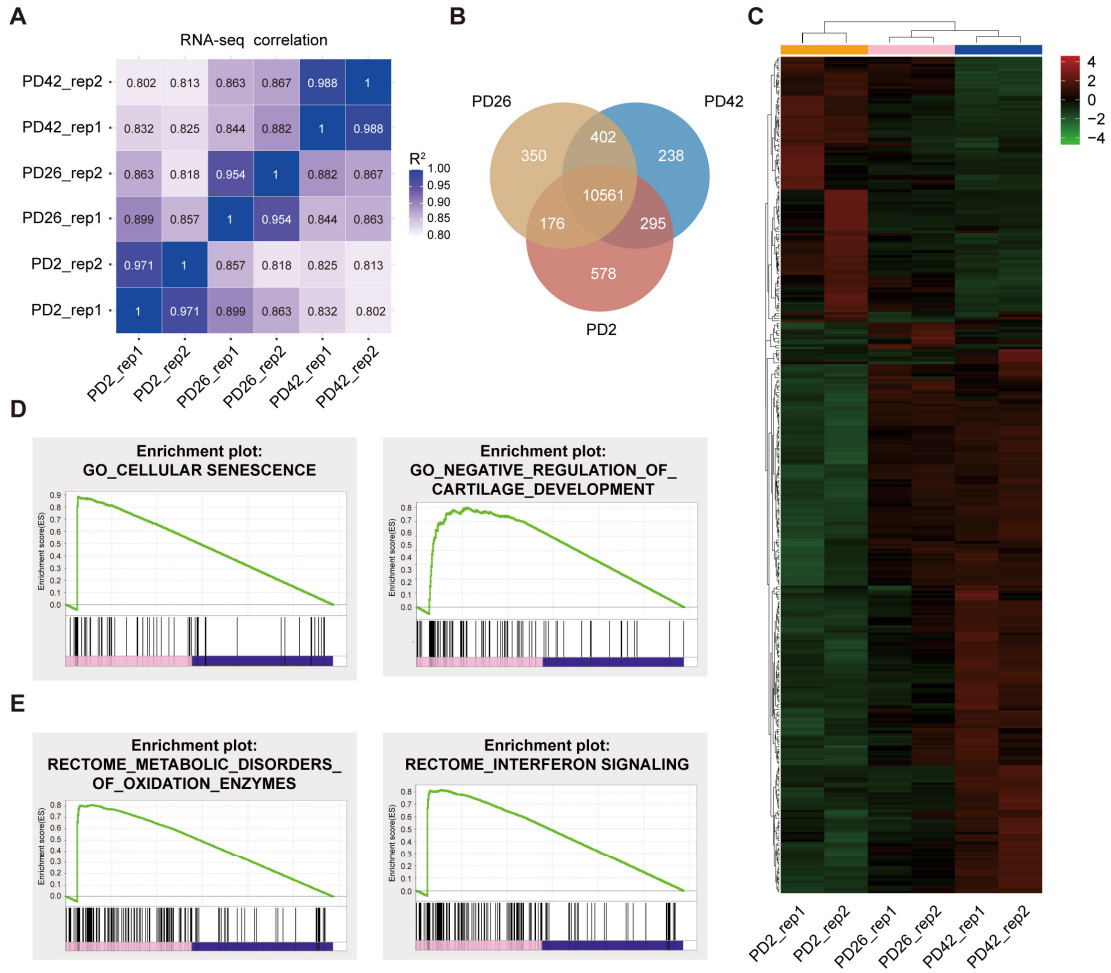

Supplementary Figure S2. Exploration of genome-wide transcriptional programs upon senescence entry. (A) Correlation heatmap of RNA-seq data. There are two independently performed biological replicates for each passage number (rep 1 and 2). (B) Venn diagram indicating the number of differentially expressed genes in in young to senescent UC-MSCs. (C) Heatmap of RNA-seq data showing hierarchically clustered gene expression in young to senescent UC-MSCs. (D, E) GSEA showing the enrichment of GO (D) and RECTOME (E) pathways in PD2 versus PD42 cells.

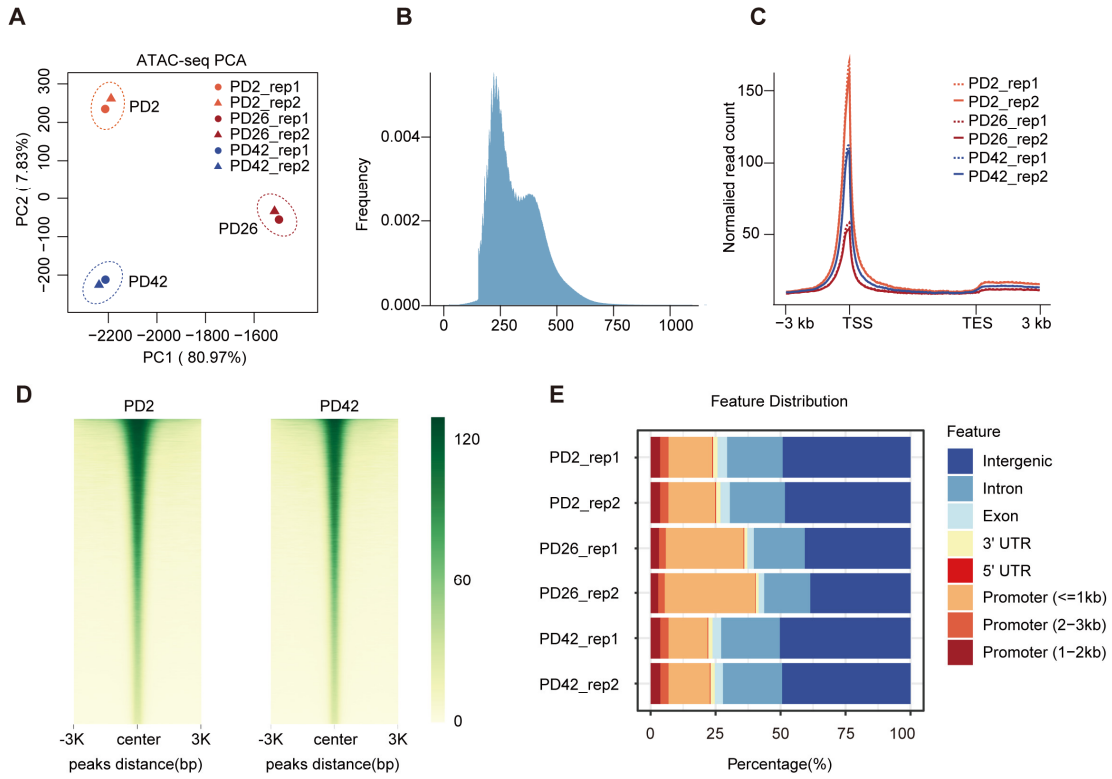

Supplementary Figure S3. Remodeling of the chromatin landscape occurs during senescence. (A) Principal Component Analysis (PCA) displaying the correlation and dispersion of ATAC-seq in young to senescent UC-MSCs. There were two independently performed biological replicates for each passage number (rep 1 and 2). (B) Representative distribution of insert size, showing clear signal modulation for mono- and di-nucleosomes. (C) Normalized ATAC-seq read count across the genome. Following peak calling, the mean ATAC-seq peaks present between the TSS (–3 kb) and the TES (+3 kb) were calculated across the genome. TSS, transcription start site; TES, transcription end site. (D) Heatmap showing normalized read densities for ATAC-seq peaks at PD2 and PD42. Tracks are centered at the peaks and extend ± 3 kb. (E) Genomic feature distributions of accessible chromatin regions that changed during senescence. UTR, untranslated region.

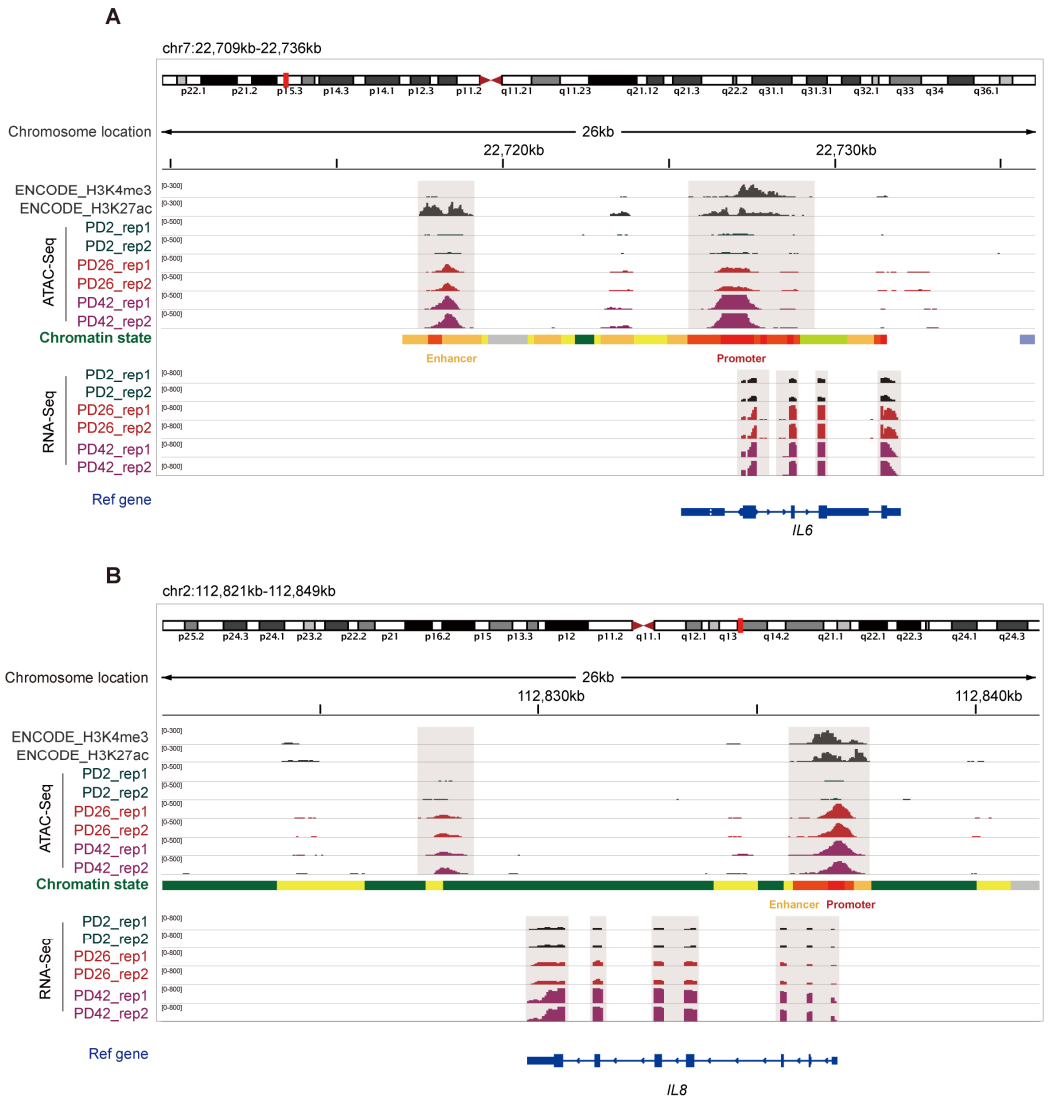

Supplementary Figure S4. ATAC-seq data are highly similar to public Encyclopedia of DNA Elements (ENCODE) data for enhancers decorated by histone modification H3K27ac. (A and B) Integrative Genomics Viewer (IGV) snapshot displaying the H3K4me3 and H3K27ac peaks of MSCs from ENCODE, in addition to our ATAC-seq and RNA-seq at the *IL6* and *IL8* loci in young to senescent UC-MSCs. Vertical gray boxes indicate enhancer and promoter ATAC-seq peaks. Chromatin states were obtained from ENCODE: yellow, weak enhancer; orange, strong enhancer; red, active promoter; green, transcribed region; and gray, heterochromatin.

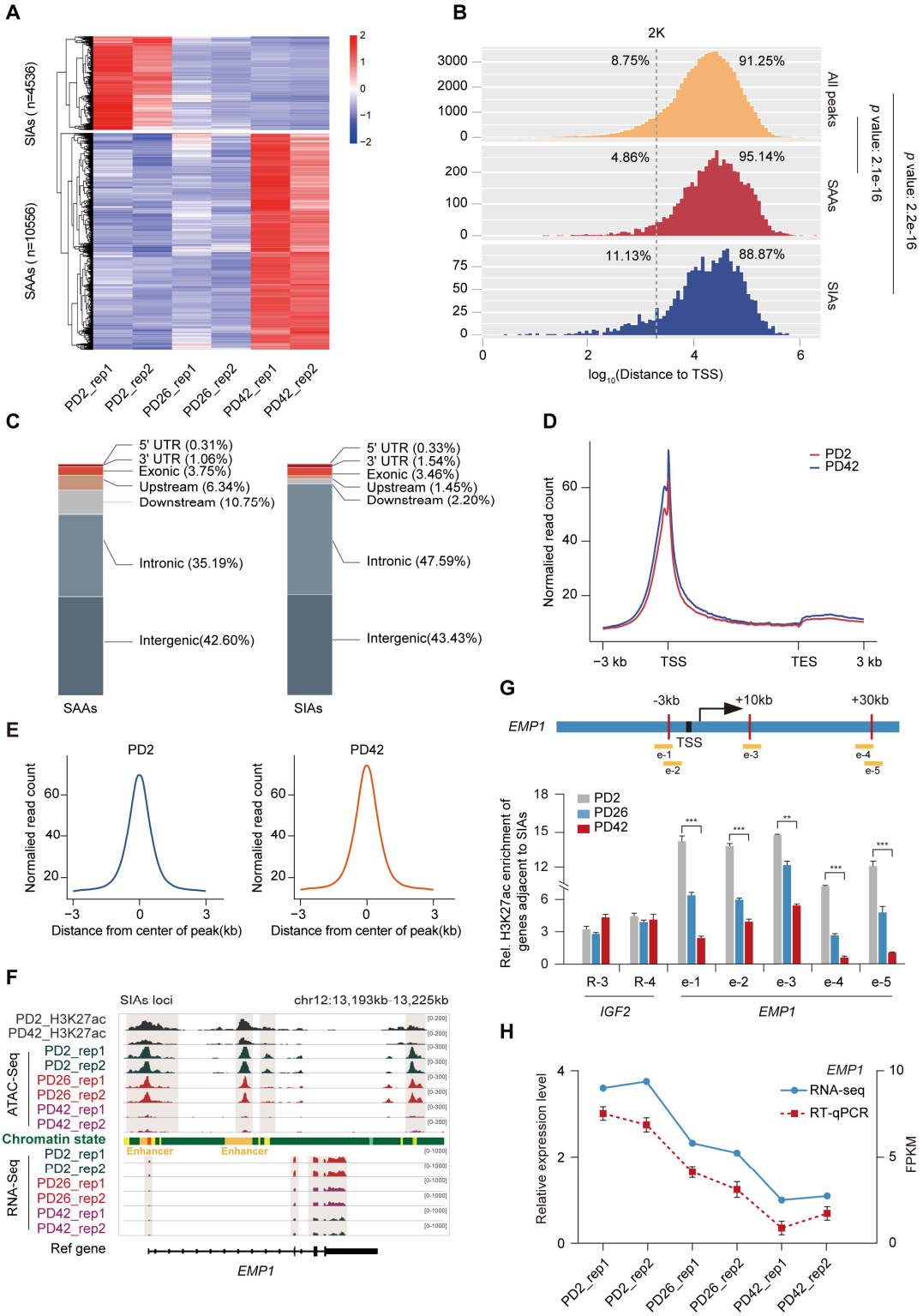

Supplementary Figure S5. Enrichment analysis of differentially accessible regions during senescence. (A) Heatmap of hierarchically clustered ATAC-seq data in young to senescent UC-MSCs displaying the remodeling of senescence-activated accessibility regions (SAAs) and senescence-inactivated accessibility regions (SIAs). (B)

Distribution of the distances between SAA or SIA ATAC-seq peaks and the TSS. (C) Annotations of SAAs and SIAs showing genomic features of the differentially accessible regions. (D) Normalized read count for the H3K27ac-driven CUT&Tag across the genome. Following peak calling, the mean H3K27ac-driven CUT&Tag peaks present between the TSS (–3 kb) and the TES (+3 kb) were calculated. (E) Enrichment of H3K27ac-driven CUT&Tag peaks at PD2 and PD42. Tracks are centered at the peaks and extend ± 3 kb. (F) Snapshot displaying the H3K27ac, ATAC-Seq, and RNA-seq profiles in young to senescent UC-MSCs at the representative SIA region of the *EMP1* locus. Vertical gray boxes indicate ATAC-seq peaks for enhancer and promoter regions and the corresponding *EMP1* expression. (G) Location diagram of H3K27ac ChIP-qPCR primers within the *EMP1* locus (top). ChIP-qPCR data showing the relative H3K27ac levels in SIAs within *EMP1* in young to senescent UC-MSCs (bottom). H3K27ac enrichment in *IGF2* was used as the positive control and IgG was used as the negative control. Enrichment was normalized to a 1:10 dilution of input. Error bars indicate the mean ± S.E.M. of three independently performed experiments. One-way ANOVA followed by Dunnett's multiple comparisons test was used for statistical analysis. N.S., not significant, $*p < 0.05$, $***p < 0.001$. (H) The expression of *EMP1* in young to senescent UC-MSCs. The dashed line indicates RT-qPCR, while the solid line indicates RNA-seq data. Error bars indicate the mean ± S.E.M. of three independently performed experiments.

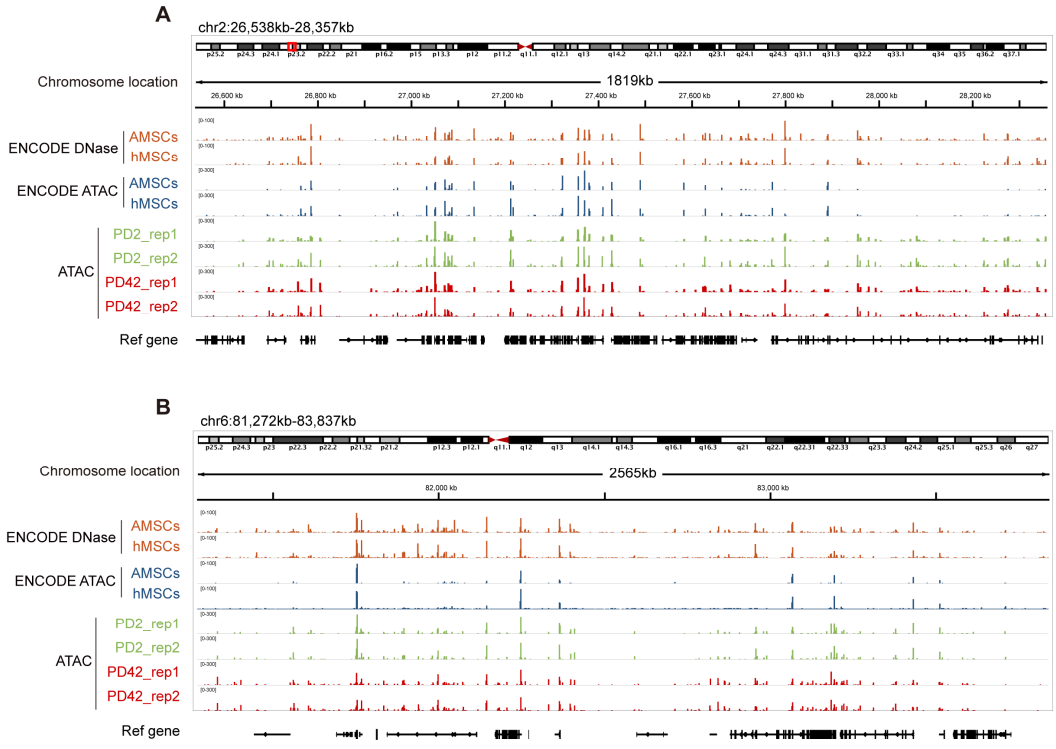

Supplementary Figure S6. Comparison between DNase-seq and ATAC-seq data from ENCODE and other types of mesenchymal stem cells and our chromatin accessibility data. (A and B) Integrative Genomics Viewer (IGV) snapshot displaying the DNase-seq and ATAC-seq peaks of AMSCs and hMSCs from ENCODE and the ATAC-seq peaks in young to senescent UC-MSCs at loci on chromosomes 2 and 6.

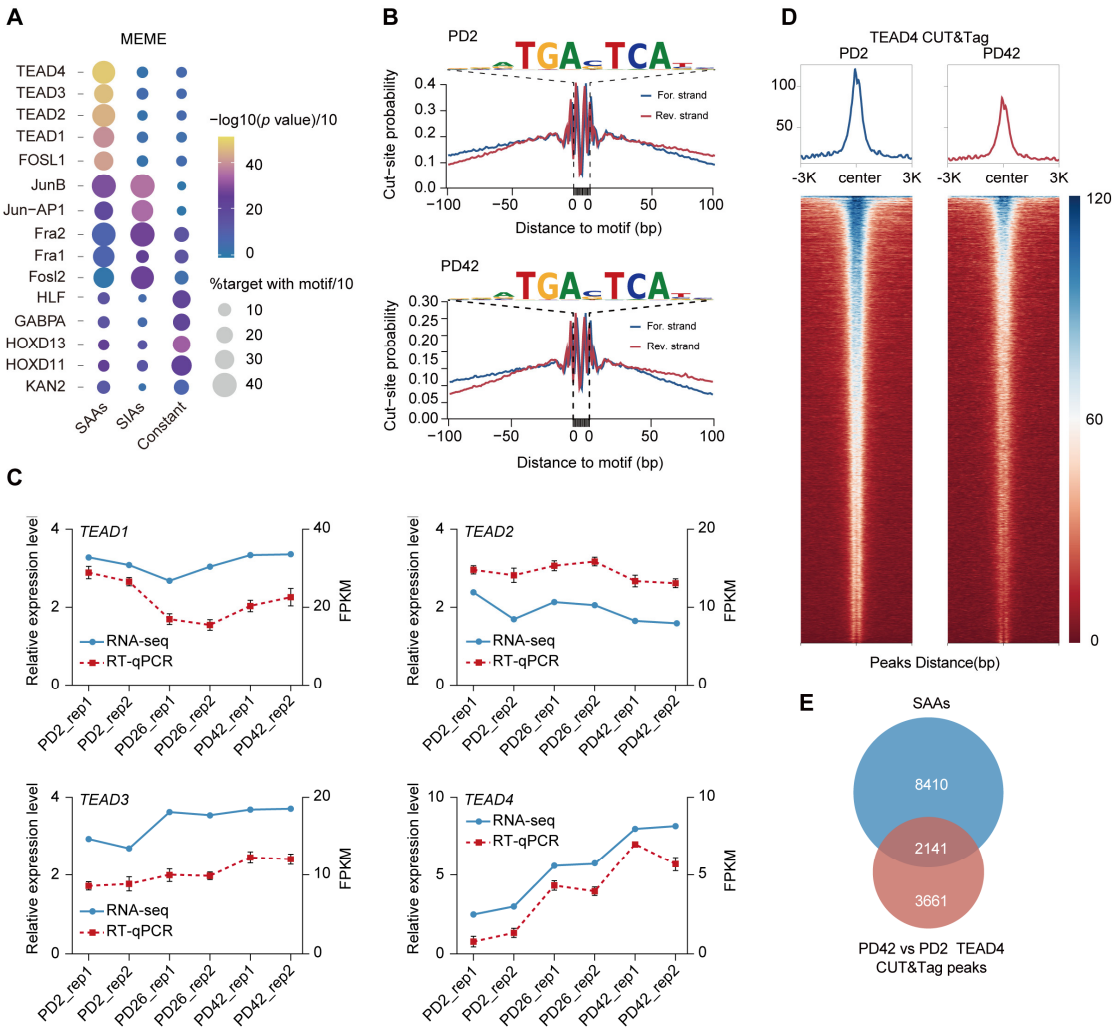

Supplementary Figure S7. TEAD4 binding at SAAs accelerates the transcription of SASP genes. (A) Top-ranked enriched motifs from MEME motif analysis of SAAs and SIAs. The circle size represents the percentage of regions with the motif and the color represents the *p* value (shrink to 10×). (B) ATAC-seq pattern in the bZIP motif at PD2 and PD42. Normalization was performed to ensure that each motif possessed the same mean number of insertions 200–500 bp away. (C) Expression of other TEAD family members, *TEAD1*, *TEAD2*, and *TEAD3* in young to senescent UC-MSCs. The dashed line indicates RT-qPCR, while the solid line indicates RNA-seq data. Error bars indicate the mean ± S.E.M. of three independently performed experiments. (D) Heatmaps and enrichment plots showing normalized read densities for TEAD4 CUT&Tag peaks performed at PD2 and PD42. Tracks are centered at the peaks and extend ± 3 kb. (E) Venn diagram showing overlap of TEAD4 CUT&Tag peaks between PD42 and PD2, in addition to SAA signals defined in ATAC-seq peaks.

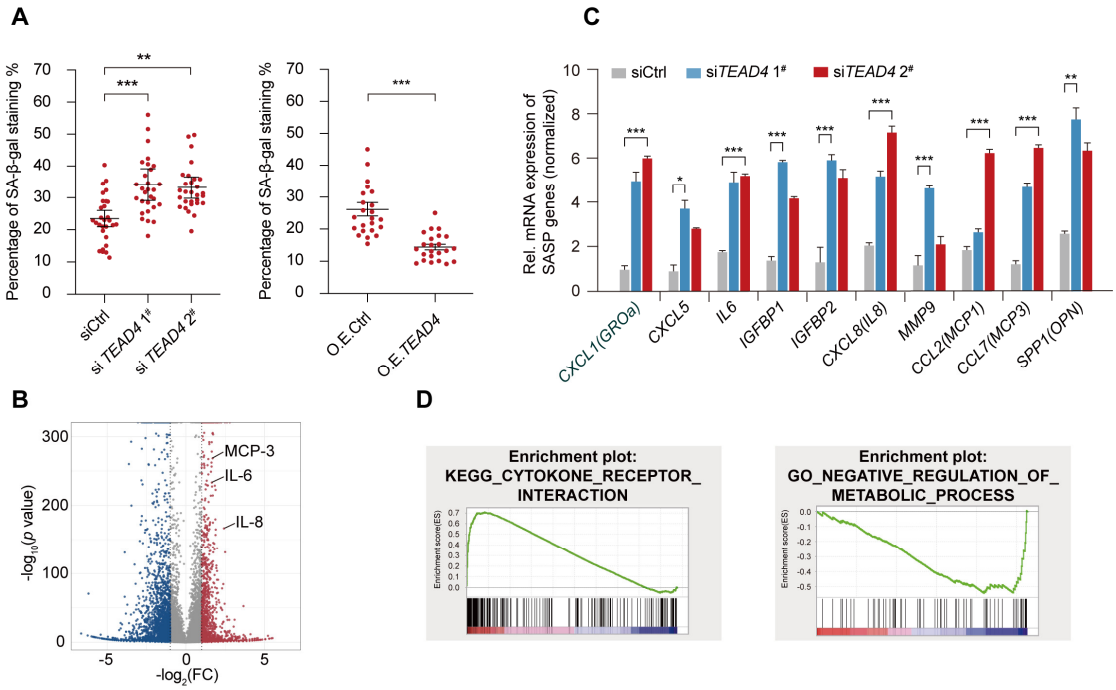

Supplementary Figure S8. Suppression of TEAD4 leads to the upregulation of SAA-adjacent SASP genes. (A) Percentage of SA-β-gal staining following TEAD4 suppression or overexpression. Scale bar, 50 μm. Error bars indicate the mean ± S.E.M. of three independently performed experiments. $^{**}p < 0.01$, $^{***}p < 0.001$. A Student's *t*-test was used for statistical analysis. (B) RNA-Seq scatter diagram showing the gene expression profiles of control versus siTEAD4 cells. Representative SASP genes are labeled. (C) RT-qPCR data showing the relative expression of SASP genes following downregulation of TEAD4 expression. Error bars indicate the mean ± S.E.M. of three independently performed experiments. $^{*}p < 0.05$, $^{**}p < 0.01$, $^{***}p < 0.001$. One-way ANOVA followed by Dunnett's multiple comparison test was used for statistical analysis. (D) GSEA showing the enrichment of SASP-related pathways in control versus siTEAD4 cells.